Received 30 December 2022; accepted 22 January 2023. Date of publication 3 February 2023; date of current version 15 February 2023.

Digital Object Identifier 10.1109/OJCOMS.2023.3240077

Performance of Wireless Powered Communication Systems Over Beaulieu-Xie Channels With Nonlinear Energy Harvesters

ADEBOLA OLUTAYO [1] (Student Member, IEEE), YANJIE DONG [2] (Member, IEEE), JULIAN CHENG [1] (Fellow, IEEE), JONATHAN F. HOLZMAN [1] (Member, IEEE), AND VICTOR C. M. LEUNG [2] (Life Fellow, IEEE)

[1]School of Engineering, The University of British Columbia, Kelowna, BC V1V 1V7, Canada

[2]Department of Electrical and Computer Engineering, The University of British Columbia, Vancouver, BC V6T 1Z4, Canada

CORRESPONDING AUTHOR: A. OLUTAYO (e-mail: adebola.olutayo@alumni.ubc.ca)

Adebola Olutayo and Yanjie Dong contributed equally to this work.

ABSTRACT Performance of wireless powered wireless systems is analyzed. The wireless devices in such systems scavenge energy from sources in downlinks and use the energy to communicate in uplinks. We introduce two new models for these energy harvesters to consider their nonlinear circuitry and their functioning over multiple line-of-sight and non-line-of-sight channels. The newly proposed Beaulieu-Xie fading model is used to characterize this manifold of channels. Performance analyses of average harvested energy and transmission outage probability show good fit between the proposed models and measured data.

INDEX TERMS Energy harvesting, communication systems, communication networks, radio frequency, performance analysis, channel modeling.

I. INTRODUCTION

ENERGY harvesting (EH) has received increasing attention because of the seamless and sustainable power that it can provide from energy sources like communication signals, solar and wind power, vibration, etc. The importance of EH can been seen in a growing number of studies across the applied sciences and engineering–on topics including piezoelectric aeroelastic EH systems [1], vibration EH systems [2], robotic/autonomous EH systems [3], and others many other systems.

In wireless communications, EH technology exploits the power of incident signals to realize wireless powered communication (WPC) [4]. These WPC systems have been studied in terms of their limited sensitivity and nonlinearity of far field radio frequency (RF) EH [5] and the detailed study of energy efficient resource allocation in wireless EH sensor network [6]. To this end, protocols have been introduced to support EH over a fraction of a timeslot and information transmission in the remainder of the timeslot [7]. The importance of EH has become critical for emerging Internet-of-Things (IoT) technology, which demands power for nodes in bodies, buildings, etc. [8], [9]. Here, EH is an attractive solution to avoid reliance on batteries.

A key challenge to the implementation of effective EH has been the characterization of its circuitry. The circuitry is typically assumed to be linear [7], [8], [9], [10], [11], [12], [13], but the constituent rectifiers and diodes, and recent experiments [14], [15], suggest that this is a poor assumption. In fact, significant performance degradation was recorded for resource allocation schemes based on linear EH models in comparison to nonlinear EH models [16]. Such deficiencies have motivated studies of nonlinear EH models like the piece-wise linear function [17], polynomial model [18], and sigmoid function [19], [20].

A second challenge has emerged through the development of high-efficiency antennas and rectifiers for millimeter-wave (mmWave) and terahertz (THz) systems [21]. These wireless communication systems have received great interest because of their ability to increase capacity beyond those in the traditional RF spectrum [22]. Such systems use emerging wireless technologies in the form of massive multiple-input multiple-output and/or small cell networks, which reduce

the propagation loss by lessening the communication distance [23]. However, their high carrier frequencies demand greater energy usage and a reliance on wireless communication over multiple line-of-sight (LOS) components plus non-line-of-sight (NLOS) components, due to their short ranges. Thus, their communication channels must be characterized by a fading model that can incorporate multiple LOS/specular and NLOS components.

Several fading models have been proposed to characterize LOS and NLOS components in wireless communication systems. The Nakagami-*m* fading model was introduced to characterize the channels in communication hops of EH systems [17], [24]. However, empirical results showed that the Nakagami-*m* fading model cannot adequately describe an environment with one or more LOS components [25]. The BX fading model overcomes this deficiency because it is derived from the noncentral chi distribution via normalization like the Nakagami-*m* fading model. This construction lets the BX fading model characterize multiple LOS components. The BX fading model also offers improved flexibility through its three fitting parameters. In fact, the BX fading model can be adapted to manifest as the existing Rayleigh, Ricean, and Nakagami-*m* fading models for appropriate parameter values.

Given the importance of nonlinearity in energy harvesters as well as the LOS/specular and NLOS components in the wireless channels, the work put forward here analyzes WPC systems operating over BX fading channels with nonlinear energy harvesters. Such work builds upon several foundational studies. These include analyses of throughput for delay-limited and delay-tolerant transmission [12], average error rate and outage probability (OP) for WPC systems with Nakagami-*m* fading channels [26], energy storage effects on OP [27], OP and average throughput of information transfer with Nakagami-*m* fading channels [28], EH-assisted overlay cognitive non-orthogonal multiple access systems with Nakagami-*m* fading channels model [29], and OP of RF EH cooperative communication systems over Nakagami-*m* fading channels [30].

In this work, we consider a WPC system where the energy harvested by the wireless device is used to transmit data to the receiver. We introduce two energy harvesters with consideration to the nonlinearity exhibited by the EH circuitry. The main contributions of this work are as follows:

- Two new nonlinear EH models are introduced and are shown to give a good fit to the measured data from [31]. The fitting is done via a best-fit search, with the goodness-of-fit quantified using root-mean square error (RMSE).
- The BX fading model is applied to characterize the fading environment with multiple LOS/specular and NLOS components. To the authors' best knowledge, this work is the first to employ the BX fading model in performance analyses of WPC networks' and the model is found to be very effective.
- Performance analyses are presented for the expectation of the harvested energy and the transmission OP while using the two newly proposed nonlinear EH models.

The paper is organized as follows. Section II presents the system model for this work. Section III shows the performance analysis of the multi-segment piecewise linear (MSPwL) EH model. Section IV presents the performance analysis of the arctangent (ArT) EH model. We present and discuss the numerical results in Section V and give concluding remarks in Section VI.

II. SYSTEM MODEL

A. VALIDITY OF THE BX MODEL FOR ENERGY HARVESTING

We consider a system for which the transfer of power occurs at a close range due to high propagation loss. These close-range systems typically function with a multitude of LOS/specular components, which cannot be effectively characterized by the existing Rayleigh, Ricean, and Nakagami-*m* fading models. The Rayleigh and Ricean fading models have limited flexibility in describing varying levels of fading [32]. The Nakagami-*m* fading model, on the other hand, can characterize a broad range of fading. However, measurements show that it can only accurately describe a fading environment with NLOS components. The BX fading model [25] was introduced to address the shortcomings of the above models. The BX fading model does so by enabling characterizations of environments with multitudes of LOS/specular and NLOS components. Moreover, the BX fading model is a generalized model that can manifest as the above Rayleigh, Ricean, and Nakagami-*m* fading models through the appropriate parameter selections.

For the BX fading model in this work, scalars and vectors are shown in lowercase letters, with the vectors in bold. The operators $\|\cdot\|$ and $\mathbb{E}[\cdot]$ denote the ℓ_2-norm and expectation of the argument, respectively. The superscript of H on a vector denotes the conjugate-transpose.

B. SYSTEM MODEL

We consider a point-to-point WPC system where a single-antenna wireless device (R) scavenges energy from an N_S-antenna energy source (S) and communicates with an N_D-antenna data fusion receiver (D) as shown in Fig. 1.

The distances between the S and R, d_1, and between R and D, d_2, are in meters. After obtaining the channel state information, $\boldsymbol{h}_{SR}$, between the energy source, S, and the wireless device, R, with $\boldsymbol{h}_{SR} \in \mathbb{C}^{N_S}$, where $\mathbb{C}^{N_S}$ is the set of all column vectors of size N_S with complex value, the energy source performs maximal-ratio transmission using the beamforming vector $\frac{\boldsymbol{h}_{SR}}{\|\boldsymbol{h}_{SR}\|}$ and transmit power p_{SR}. Therefore, the received signal at the wireless device, R, is

$$y_S = \|\boldsymbol{h}_{SR}\|_2 \sqrt{p_{SR}} x_{SR} + z_S \tag{1}$$

where x_{SR} is the transmitted signal, and z_S is additive white Gaussian noise (AWGN) with zero mean and a variance

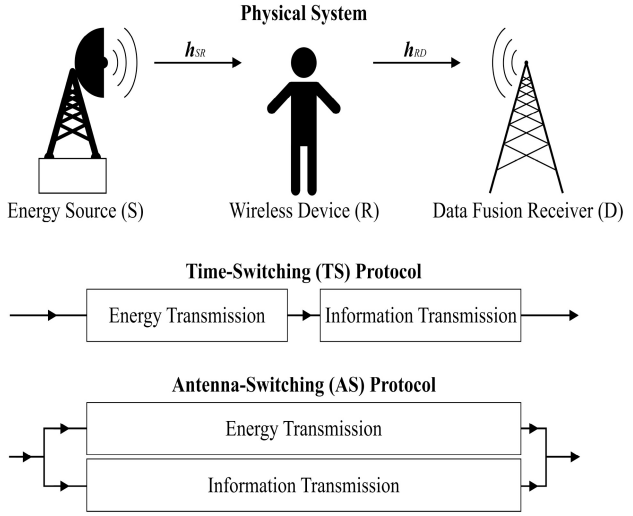

FIGURE 1. The system model is shown as the physical system, with channel state information h_{SR} and h_{RD} from the energy source (S) to the wireless device (R) and then the data fusion receiver (D), the time-switching (TS) protocol, and the antenna-switching (AS) protocol.

of σ_S^2. The wireless device, R, harvests energy from the signal giving a usable power of

$$P_{RD} = \varpi P_{EH}^{\phi}\left(p_{SR}\|\boldsymbol{h}_{SR}\|^2\right) \tag{2}$$

where P_{EH}^{ϕ} represents the energy harvested, ϕ represents the energy harvester model, and ϖ denotes the switching protocol, such as the time-switching (TS) protocol [17] and antenna-switching (AS) protocol [17]. After the maximal-ratio combining via $\frac{\boldsymbol{h}_{RD}}{\|\boldsymbol{h}_{RD}\|}$, the received signal at the data fusion receiver, D, is

$$y_D = \|\boldsymbol{h}_{RD}\|_2\sqrt{P_{RD}}x_{RD} + \frac{\boldsymbol{h}_{RD}^H}{\|\boldsymbol{h}_{RD}\|}z_D \tag{3}$$

where $\boldsymbol{h}_{RD} \in \mathbb{C}^{N_D}$ is the complex channel coefficient vector, and $\boldsymbol{z}_D \in \mathbb{C}^{N_D}$ is AWGN with zero mean and a covariance of $\sigma_D^2\boldsymbol{I}_{N_D}$, where $\boldsymbol{I}_{N_D}$ is a unity matrix. Therefore, the received signal-to-noise (SNR) at the data fusion receiver, D is

$$\gamma_D = \frac{P_{RD}\|\boldsymbol{h}_{RD}\|^2}{\sigma_D^2} \tag{4}$$

where σ_D^2 is the noise power.

C. NONLINEAR ENERGY HARVESTER MODELS

In this work, we consider two EH models: the multi-segment piecewise linear (MSPwL) energy harvester and the arctangent (ArT) energy harvester.

1) MULTI-SEGMENT PIECEWISE LINEAR ENERGY HARVESTER

The MSPwL energy harvester approximates its input-output relation with linear segments. We consider an MSPwL energy harvester with N segments of input-output

$$P_{EH}^{MSPwL}\left(p_{SR}\|\boldsymbol{h}_{SR}\|^2\right) = a_n p_{SR}\|\boldsymbol{h}_{SR}\|^2 + b_n,$$
$$c_{n-1} \le p_{SR}\|\boldsymbol{h}_{SR}\|^2 \le c_n \tag{5}$$

where $a_n \ge 0$ and b_n are the slope and intercept of the nth segment, respectively. Here, $b_n = \sum_{k=1}^{n-1}(a_k - a_{k+1})c_k + b_1$, with $b_1 = 0$, $n = 2, 3, \ldots, N$, and $0 = c_0 < c_1 < \ldots < c_N = \infty$.

2) ARCTANGENT ENERGY HARVESTER

The ArT energy harvester approximates its input-output relation by an arctangent function as

$$P_{EH}^{ArT}\left(p_{SR}\|\boldsymbol{h}_{SR}\|^2\right) = a_0\tanh\left(b_0 p_{SR}\|\boldsymbol{h}_{SR}\|^2\right) \tag{6}$$

where $a_0 \ge 0$ and $b_0 \ge 0$ are the two key parameters.

D. REVIEW OF THE BX FADING MODEL

We consider a BX random variable (RV), Y, which is derived from the noncentral chi RV via normalization [22], [25]. The distribution of $X = |Y|^2$ is noncentral chi-squared, i.e., $\chi^2(2m, \frac{2m}{\Omega}\lambda^2)$, and it has a complementary cumulative distribution function (CCDF) of

$$F_X^c(x) = Q_m\left(\lambda\sqrt{\frac{2m}{\Omega}}, \sqrt{\frac{2mx}{\Omega}}\right) \tag{7}$$

where m is the fading parameter, λ^2 is the power of the LOS component(s), Ω is the power of the NLOS components, $I_v(\cdot)$ is the vth-order modified Bessel function of the first kind, and $Q_m(\cdot,\cdot)$ is the Marcum Q-function [33]. Hence, the distributions of $\|\boldsymbol{h}_{SR}\|^2$ and $\|\boldsymbol{h}_{RD}\|^2$ are $\chi^2(2m_1N_S, \frac{2m_1}{\Omega_{SR}}\lambda_{SR}^2)$ and $\chi^2(2m_2N_D, \frac{2m_2}{\Omega_{RD}}\lambda_{RD}^2)$, respectively, where m_1, λ_{SR}^2, and Ω_{SR} are the fading severity parameter, power of the LOS component(s), and power of the NLOS components of the S-R link, respectively, while m_2, λ_{RD}^2, and Ω_{RD} are the fading severity parameter, power of the LOS component(s), and power of the NLOS components of the R-D link, respectively. Note that λ_{SR}^2 and λ_{RD}^2 can be obtained via the relations $\lambda_{SR}^2 = \sum_{l=1}^{N_S}\lambda_l^2$ and $\lambda_{RD}^2 = \sum_{j=1}^{N_D}\lambda_j^2$, respectively, where λ_l^2 and λ_j^2 are the powers of the LOS component per branch in the S-R and R-D links, respectively.

E. PERFORMANCE METRICS

We consider the performance metrics of expected EH rate (EEHR) and transmission outage probability (TOP). The EEHR is defined as

$$\overline{P_{RD}} = \mathbb{E}[P_{RD}]. \tag{8}$$

Based on (3), the information rate between the wireless device, R, and the data fusion receiver, D, is denoted by

$$R_D = \varrho W\log\left(1 + \frac{\gamma_D}{\varrho}\right) \tag{9}$$

where W is the system bandwidth, and ϱ is specified by the switching protocol under study. Ultimately, the parameters

ϖ and ϱ are factors that denote the EH architecture. The case with $\varpi = 1$ and $\varrho = 1$ corresponds to the AS protocol, while the case with $\varpi = \rho$ and $\varrho = 1 - \rho$ corresponds to the TS protocol with $\rho \in [0, 1]$. Thus, the TOP, which is defined as the probability that the transmission rate falls below a predefined threshold, can be expressed as

$$\begin{aligned} P_{out} &= \Pr\{R_D \le R_{req}\} \\ &= \Pr\left\{\|\boldsymbol{h}_{RD}\|^2 \le \frac{\varrho\sigma_D^2}{P_{RD}}\left[\exp\left(\frac{R_{req}}{\varrho W}\right) - 1\right]\right\} \end{aligned} \tag{10}$$

where R_{req} is a predefined threshold.

III. PERFORMANCE OF WPC WITH THE MULTI-SEGMENT PIECEWISE LINEAR ENERGY HARVESTER

A. EXPECTED ENERGY HARVESTING RATE

In this section, we analyze the EEHR for the MSPwL energy harvester. We express the EEHR as

$$\overline{P_{RD}} = \mathbb{E}[P_{RD}] = \Pr\{P_{RD} > x\} = \int_0^\infty F_{RD}^c(x)dx \tag{11}$$

where the CCDF of P_{RD} is derived in Appendix A to give (26). Inserting (26) into (11) gives the EEHR as

$$\overline{P_{RD}} = \int_{\varpi d_{i-1}}^{\varpi d_i} Q_{N_S m_1}\left(\lambda_{SR}\sqrt{\frac{2m_1}{\Omega_{SR}}}, A\right)dx \tag{12}$$

where $A = \sqrt{\frac{2m_1}{a_i p_{SR}\Omega_{SR}}(\frac{x}{\varpi} - b_i)}$. Applying the series expression of the Marcum Q-function [33] and an identity of the modified Bessel function of the first kind [34, p. 919] to (12), we obtain the EEHR as

$$\begin{aligned} \overline{P_{RD}} = \exp&\left[-\frac{m_1}{\Omega_{SR}}\left(\lambda_{SR}^2 - \frac{b_i}{a_i p_{SR}}\right)\right]\sum_{q=1-m_1N_S}^{\infty} \\ &\times \sum_{w=0}^{\infty}\frac{1}{w!\Gamma(w+q+1)}\left(\frac{m_1}{\Omega_{SR}}\right)^{2w+q}\lambda_{SR}^{2q+2w}(a_i\varpi p_{SR})^{-w} \\ &\times \int_{\varpi d_{i-1}}^{\varpi d_i}(x - \varpi b_i)^w \exp\left(-\frac{m_1}{\Omega_{SR}}\left(\frac{x}{a_i\varpi p_{SR}}\right)\right)dx. \end{aligned} \tag{13}$$

B. TRANSMISSION OUTAGE PROBABILITY

Here, we analyze the TOP for the MSPwL energy harvester. As expressed in (10), the TOP is defined as

$$\begin{aligned} P_{out} &= \Pr\{R_D \le R_{req}\} = \Pr\left\{P_{RD} \le \frac{\varepsilon}{\|\boldsymbol{h}_{RD}\|^2}\right\} \\ &= 1 - \int_0^{P_{\max}} \frac{1}{\varepsilon} f_{\frac{1}{\|\boldsymbol{h}_{RD}\|^2}}\left(\frac{x}{\varepsilon}\right) F_{p_{RD}}^c(x)dx \end{aligned} \tag{14}$$

where $\varepsilon \triangleq \sigma_D^2\varrho\left[\exp(\frac{R_{req}}{\varrho W}) - 1\right]$. The CDF of $\frac{1}{\|\boldsymbol{h}_{RD}\|^2}$ based on (7) is

$$\begin{aligned} F_{\frac{1}{\|\boldsymbol{h}_{RD}\|^2}}(p) &= \Pr\left\{\frac{1}{\|\boldsymbol{h}_{RD}\|^2} \le p\right\} = \Pr\left\{\|\boldsymbol{h}_{RD}\|^2 \ge \frac{1}{p}\right\} \\ &= Q_{m_2N_D}\left(\lambda_{RD}\sqrt{\frac{2m_2}{\Omega_{RD}}}, \sqrt{\frac{2m_2}{\Omega_{RD}p}}\right). \end{aligned} \tag{15}$$

The PDF of $\frac{1}{\|\boldsymbol{h}_{RD}\|^2}$ is obtained by taking the first-order derivative of (15) as [33]

$$\begin{aligned} f_{\frac{1}{\|\boldsymbol{h}_{RD}\|^2}}(p) = &\frac{m_2}{\Omega_{RD}}\lambda_{RD}^{1-N_Dm_2} \times I_{N_Dm_2-1}\left(\frac{2m_2\lambda_{RD}}{\Omega_{RD}\sqrt{p}}\right) \\ &\times \left(\frac{1}{p}\right)^{\frac{N_Dm_2+3}{2}}\exp\left(-\frac{m_2}{\Omega_{RD}}\left(\lambda_{RD}^2 + \frac{1}{p}\right)\right). \end{aligned} \tag{16}$$

Substituting (16) and (26) into (14) then gives the TOP as

$$\begin{aligned} P_{out} = 1 - &\sum_{i=1}^{N-1}\frac{m_2}{\Omega_{RD}}\varepsilon^{\frac{N_Dm_2+1}{2}}\lambda_{RD}^{1-N_Dm_2}\exp\left(-\frac{m_2}{\Omega_{RD}}\lambda_{RD}^2\right) \\ &\times \int_{\varpi d_{i-1}}^{\varpi d_i}\left(\frac{1}{x}\right)^{\frac{N_Dm_2+3}{2}} I_{N_Dm_2-1}\left(\frac{2m_2\lambda_{RD}\sqrt{\varepsilon}}{\Omega_{RD}\sqrt{x}}\right) \\ &\times Q_{N_Sm_1}\left(\lambda_{SR}\sqrt{\frac{2m_1}{\Omega_{SR}}}, A\right)\exp\left(-\frac{m_2\varepsilon}{\Omega_{RD}x}\right)dx. \end{aligned} \tag{17}$$

Applying the series expression of the Marcum Q-function [33] and an identity of the modified Bessel function of the first kind [34, p. 919] to (17), we have

$$\begin{aligned} P_{out} = 1 - &\sum_{i=1}^{N-1}\exp\left(-\frac{m_1}{\Omega_{SR}}\lambda_{SR}^2 - \frac{m_2}{\Omega_{RD}}\lambda_{RD}^2\right)\sum_{q=1-m_1N_S}^{\infty} \\ &\times \sum_{w=0}^{\infty}\frac{1}{w!\Gamma(w+m_2N_D)}\sum_{s=0}^{\infty}\frac{1}{s!\Gamma(s+q+1)}\varepsilon^{w+N_Dm_2} \\ &\times \left(\frac{m_1}{\Omega_{SR}}\right)^{2s+q}\left(\lambda_{SR}^2\right)^{s+q}(a_ip_{SR})^{-s}\left(\frac{m_2}{\Omega_{RD}}\right)^{2w+m_2N_D} \\ &\times \int_{\varpi d_{i-1}}^{\varpi d_i}\left(\frac{1}{x}\right)^{w+N_Dm_2+1}\left(\frac{x}{\varpi} - b_i\right)^s\exp\left(-\frac{m_2\varepsilon}{\Omega_{RD}x}\right) \\ &\times \lambda_{RD}^{2w}\exp\left(-\frac{m_1}{a_i\Omega_{SR}p_{SR}}\left(\frac{x}{\varpi} - b_i\right)\right)dx. \end{aligned} \tag{18}$$

These final results for the $\overline{P_{RD}}$ and P_{out} both contain one integral, which can be solved using standard mathematical software such as MATLAB or Mathematica.

IV. PERFORMANCE OF WPC WITH THE ARCTANGENT ENERGY HARVESTER

A. EXPECTED ENERGY HARVESTING RATE FOR ART

The EEHR is defined for the ArT energy harvester via (11) while the CCDF of P_{RD} is derived in Appendix B to yield (28). Inserting (28) into (11) gives

$$\overline{P_{RD}} = \int_0^\infty Q_{m_1N_S}\left(\lambda_{SR}\sqrt{\frac{2m_1}{\Omega_{SR}}}, \sqrt{\frac{m_1B}{b_0p_{SR}\Omega_{SR}}}\right)dx \tag{19}$$

where $B = \ln(\frac{a_0\varpi + x}{a_0\varpi - x})$. Applying the series expression of the Marcum Q-function [33] and an identity of the modified Bessel function of the first kind [34, p. 919] to (19), we obtain the EEHR expression as

$$\overline{P_{RD}} = \exp\left(-\frac{m_1\lambda_{SR}^2}{\Omega_{SR}}\right)\sum_{q=1-m_1N_S}^{\infty}\sum_{w=0}^{\infty}\frac{1}{w!\Gamma(w+q+1)} \times \left(\frac{2}{b_0 p_{SR}}\right)^w\left(\lambda_{SR}^2\right)^{w+q}\left(\frac{m_1}{\Omega_{SR}}\right)^{2w+q} \times \int_0^{\infty} B^w \exp\left(-\frac{m_1 B}{b_0 p_{SR}\Omega_{SR}}\right)dx. \quad (20)$$

B. TRANSMISSION OUTAGE PROBABILITY FOR ART

The TOP is defined for the ArT model as

$$P_{out} = 1 - \int_0^{\pi a_0 \varpi} \frac{1}{\varepsilon} f_{\frac{1}{\|h_{RD}\|^2}}\left(\frac{x}{\varepsilon}\right) F_{p_{RD}}^c(x)dx. \quad (21)$$

Substituting (16) and (28) into (21) then gives

$$P_{out} = 1 - \frac{m_2}{\Omega_{RD}}\varepsilon^{\frac{N_D m_2+1}{2}}\lambda_{RD}^{1-N_D m_2} \times \exp\left(-\frac{m_2}{\Omega_{RD}}\lambda_{RD}^2\right) \times \int_0^{\pi a_0 \varpi}\left(\frac{1}{x}\right)^{\frac{N_D m_2+3}{2}} \times I_{N_D m_2-1}\left(\frac{2m_2\lambda_{RD}\sqrt{\varepsilon}}{\Omega_{RD}\sqrt{x}}\right) \times \exp\left(-\frac{m_2\varepsilon}{\Omega_{RD}x}\right) Q_{N_S m_1}\left(\lambda_{SR}\sqrt{\frac{2m_1}{\Omega_{SR}}}, \sqrt{\frac{m_1 B}{b_0 p_{SR}\Omega_{SR}}}\right)dx. \quad (22)$$

Applying the series expression of the Marcum Q-function [33] and an identity of the modified Bessel function of the first kind [34, p. 919] to (22) gives

$$P_{out} = 1 - \exp\left(-\frac{m_1}{\Omega_{SR}}\lambda_{SR}^2 - \frac{m_2}{\Omega_{RD}}\lambda_{RD}^2\right)\sum_{q=1-m_1N_S}^{\infty} \times \sum_{w=0}^{\infty}\frac{1}{w!\Gamma(w+m_2N_D)}\sum_{s=0}^{\infty}\frac{1}{s!\Gamma(s+q+1)}\left(\frac{m_1}{\Omega_{SR}}\right)^{2s+q} \times \lambda_{SR}^{(2s+2q)}(2b_0p_{SR})^{-s}\left(\frac{m_2}{\Omega_{RD}}\right)^{2w+N_Dm_2}\lambda_{RD}^{2w} \times \varepsilon^{w+N_Dm_2} \times \int_0^{a_0\varpi}\left(\frac{1}{x}\right)^{w+N_Dm_2+1} B^s \times \exp\left(-\frac{m_1 B}{2b_0\Omega_{SR}p_{SR}}\right) \times \exp\left(-\frac{m_2\varepsilon}{\Omega_{RD}x}\right)dx. \quad (23)$$

The final results for the $\overline{P_{RD}}$ and P_{out} both contain one integral, which can be solved using standard mathematical software such as MATLAB or Mathematica.

V. NUMERICAL RESULTS

In this section, we fit the MSPwL and ArT energy harvesters to measurement data [31]. The measurement data is obtained from an experiment that measures the performance of a RF-DC power conversion system having (wireless) electromagnetic wave radiation as its input. The output of the signal generator is amplified to generate signals with a power of 6 W at a frequency range of 902–928 MHz. The signal at the output of the power amplifier is then fed to an antenna, which emits an equivalent isotropically radiated power up to a maximum of 4 W. The measured data shows the output power as a function of received power for different load resistances. The results from performance analyses of the average harvested energy and TOP are shown in Figs. 2–4 for the energy harvesters introduced in Sections III and IV.

TABLE 1. Fitted parameters to measured data [31, Fig. 17d] for a load resistance of 5.6 MΩ with MSPwL and ArT energy harvesters.

EH model	a_n	b_n	RMSE
2-segment MSPwL	0.1317, 0.0042	0, 7.372×10^{-6}	1.21×10^{-6}
3-segment MSPwL	0.3990, 0.0389, 5.515×10^{-4}	0, 2.9136×10^{-6}, 1.0086×10^{-5}	9.56×10^{-8}
4-segment MSPwL	0.3990, 0.0427, 0.0018, 2.34×10^{-4}	0, 2.6964×10^{-6}, 9.6167×10^{-6}, 1.0366×10^{-5}	5.15×10^{-8}
ArT	1.079×10^{-5}	7.90×10^{3}	7.52×10^{-7}

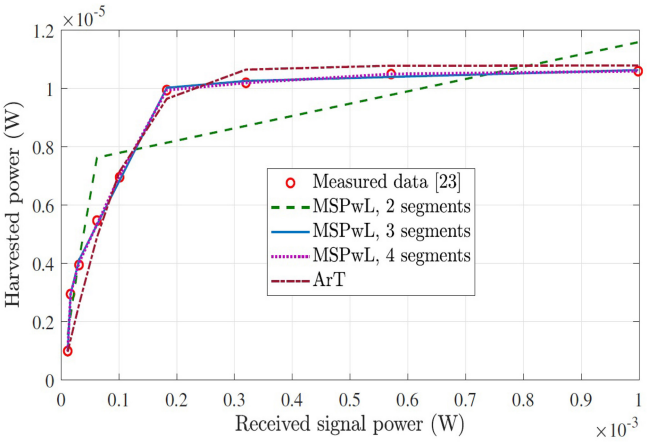

FIGURE 2. Fits of the harvested power for MSPwL and ArT energy harvesters to measured data from [31, Fig. 17d] as a function of the transmit power for a 5.6 MΩ load resistance. The RMSE values for the 2-, 3-, and 4-segment MSPwL energy harvesters are 1.21×10^{-6}, 9.56×10^{-8}, and 5.15×10^{-8}, respectively. The RMSE value for the ArT energy harvester is 7.52×10^{-7}.

Fig. 2 shows fits of the harvested power for the MSPwL and ArT energy harvesters to measured data from [31, Fig. 17d] versus transmit power for a load resistance of 5.6 MΩ. For the MSPwL energy harvester, we consider 2, 3, and 4 segments. The parameters were obtained via a best-fit search to the measured data with the goodness-of-fit quantified by root mean square error (RMSE). Table 1 shows the parameter values for 2-, 3-, 4-segment MSPwL and ArT energy harvesters. The deviation of the curves of the MSPwL and ArT energy harvesters from the measured data is quantified by the RMSE values shown in Table 1. We observe that the 4-segment MSPwL energy harvester provides the best fit. This is expected as we can see from the input-output relations of the energy harvesters in (5) and (6) that the curve of the ArT energy harvester is largely dependent on the arctangent function, which is not true for MSPwL energy harvester. We also observe that the ArT energy harvester offers an improved fit over the 2-segment MSPwL energy harvester, but this changes as the number of segments in MSPwL increases. More importantly, we see that both of our energy harvesters give improved fit over the EH models [24, Fig. 1a] using the same experimental. In the paragraphs that follow, we apply the values of out parameters from the fitting in Fig. 2 to simulate the average

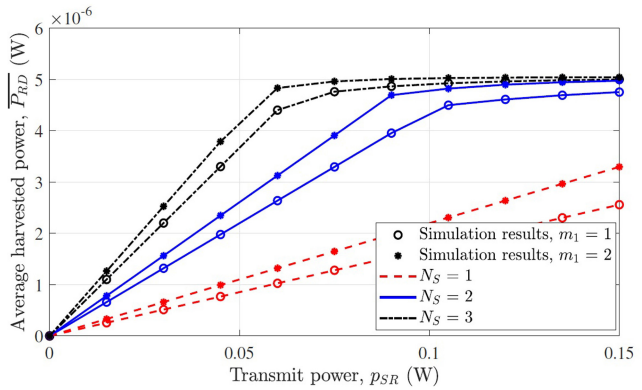

FIGURE 3. Curves for the average harvested power, $\overline{P_{RD}}$, versus transmit power, p_{SR}, for a 3-segment MSPwL energy harvester at a distance of $d_1 = 10$ m with a pathloss exponent of $s_1 = 2$, unity-gain antennas, a parameter value of $\varpi = 0.5$, and different values of m_1 and N_S. The parameters a_n and b_n have the values [0.3990 0.0389 5.515 × 10^{-4}] and [0 2.9136 × 10^{-6} 1.0086 × 10^{-5}], respectively.

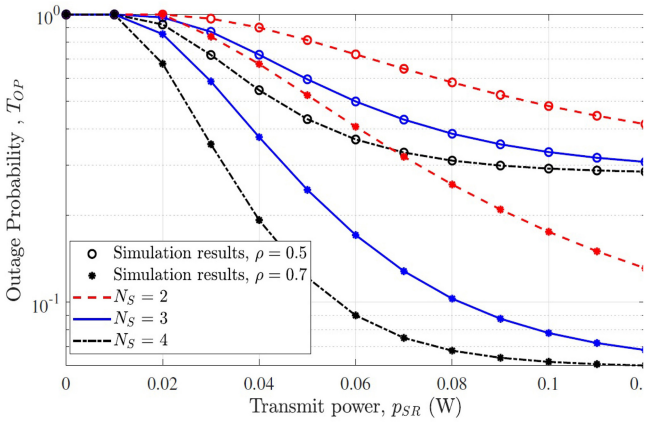

FIGURE 4. The TOP curves versus transmit power, p_{SR}, for the 3-segment MSPwL energy harvester for parameters values of $m_1 = m_2 = 2$, $N_D = 2$, a_n = [0.3990 0.0389 5.515 × 10^{-4}], and b_n = [0 2.9136 × 10^{-6} 1.0086 × 10^{-5}].

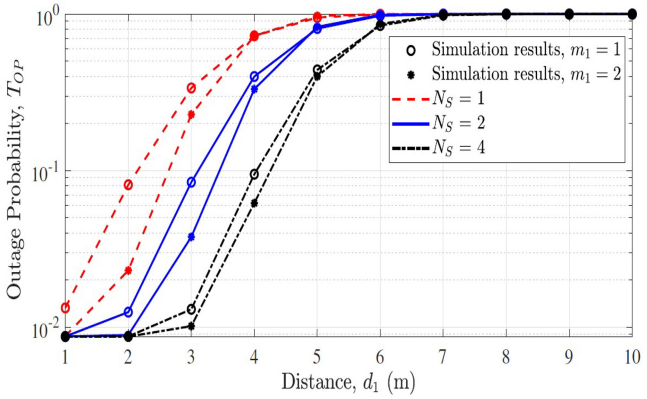

FIGURE 5. The TOP curves for the ArT energy harvester versus distance, d_1, for a transmit power, p_{SR}, of 100 mW and parameters values of $m_2 = 2$, $N_D = 2$, $\varpi = \varrho = 0.5$, $a_0 = 1.079 \times 10^{-5}$, and $b_0 = 7.90 \times 10^3$.

harvested power and TOP for 3-segment MSPwl and ArT energy harvesters.

Fig. 3 shows the average harvested power, $\overline{P_{RD}}$, for a 3-segment MSPwL energy harvester. The curves display $\overline{P_{RD}}$ versus transmit power, p_{SR}, of the energy source, S, at a distance, $d_1 = 10$ m with a pathloss exponent of $s_1 = 2$ and unity-gain antennas. The simulation uses parameter values of $\varpi = 0.5$ and different values of m_1 and N_S. The energy harvester has the parameters a_n and b_n take on values of [0.3990 0.0389 5.515×10^{-4}] and [0 2.9136×10^{-6} 1.0086×10^{-5}], respectively. We observe that all the curves start to roll-off from linear to nonlinear for higher values of transmit power, p_{SR}. This characteristic follows that shown by experimental results shown in Fig. 2. Also, when the fading parameter m_1 is increased from 1 to 2, the harvested power increases. However, the increase in harvested power becomes less significant as it approaches the saturation level of the EH circuit, even for an increased value of N_S. Overall, we see that less severe fading in the first hop gives more harvested power. Moreover, increasing the number of energy beamforming antennas, N_S, does not increase the harvested power above the saturation level of the EH circuit.

Fig. 4 shows TOP curves for a 3-segment MSPwL energy harvester over BX fading channels versus transmit power, p_{SR}. This simulation is obtained by considering the TS protocol for different values of ρ and different numbers of energy beamforming antennas, N_S. The number of data fusion receiver antennas, N_D, is 2, and the fading parameters m_1 and m_2 both take on values of 2. The parameter a_n has values of [0.3990 0.0389 5.515×10^{-4}], while the parameter b_n has values of [0 2.9136×10^{-6} 1.0086×10^{-5}]. The value of the expression $\frac{R_{req}}{\varrho W}$ is 0.2, while the distances d_1 and d_2 are both 10 m, with a pathloss exponent of 2. We observe that the P_{out} curves exhibit an outage floor as the transmit power, p_{SR}, increases, which is due to the saturation level of the EH circuit. In particular, we observe that as the number of energy beamforming antennas, N_S, increases, the outage floor is attained at a lower transmit power, p_{SR}. The effect of increasing the value of ρ from 0.5 to 0.7 is seen to improve the TOP values. However, the significance of the improvement reduces as N_S increases. Again, this is due to the saturation level of the EH circuit.

Fig. 5 shows TOP curves for the ArT energy harvester versus the distance, d_1, with a pathloss exponent of 2 and a transmit power, p_{SR}, of 100 mW for differing numbers of energy beamforming antenna, N_S, and differing values of the fading parameter, m_1. The number of data fusion receiver antennas is $N_D = 2$, the fading parameter is $m_2 = 2$, the distance is $d_2 = 8$ m, with a pathloss exponent of 2, the TS protocol parameters are $\varpi = \varrho = 0.5$, and the parameters a_0 and b_0 are 1.079×10^{-5} and 7.90×10^3, respectively. The expression $\frac{R_{req}}{\varrho W}$ takes on a value of 0.1. Note that the distance between the wireless device, R, and the data fusion receiver, D, remains unchanged at 8 m. From the curves, we see that the outage improves when the fading parameter m_1, increases from 1 to 2 (to indicate less severe fading). Also, increasing the number of diversity branches leads to improved outage

performance. Ultimately, we see that the WPC system attains better performance when the wireless device is close to the energy source, as expected.

Our simulation results present performance analyses of the WPC system, whose channel is described by the BX fading models. These results can present new insights into the wireless communication protocols at the physical, data link, and network layers, which can ultimately guide the development of new communication technologies.

VI. CONCLUSION

We analyzed the average harvested energy and TOP of WPC systems via two newly-proposed nonlinear EH models. Fading was considered to be BX distributed because of the (often present) multitude of LOS and NLOS components. Our results showed that the EH circuitry of both models exhibits saturation levels as the transmit power increases. The results also showed the effects of increasing the number of energy beamforming antennas, fading parameter, distance, and harvesting time (as seen by the TS protocol parameters) on the average harvested energy and TOP. We observed that increasing the number of energy beamforming antenna reduces the transmit power for a set outage floor. Also, increasing the EH time leads to an improved outage. However, the improvement becomes less significant as the number of energy beamforming antennas increases. Ultimately, the two newly-introduced nonlinear energy harvesters showed good fits to measure data in terms of average harvested energy and TOP. Future works employing the BX fading model and our EH models can further investigate the effect of TS and AS protocols on the performance of WPC systems. In addition, our new EH models can be studied for secure cooperative communication network, simultaneous wireless information and power transfer systems, resource allocation, and full-duplex communication systems.

APPENDIX A
PROOF OF CCDF FOR MSPWL

The CCDF of the transmission power of sensor, P_{RD}, is

$$F^c_{P_{RD}}(x) = \Pr\left\{\varpi P^{MSPwL}_{EH}\left(p_{SR}\|\boldsymbol{h}_{SR}\|^2 \geq x\right)\right\}. \quad (24)$$

First, we define an interval $[d_{i-1}, d_i]$ with $d_0 = 0$, $d_N = d_{N-1}$, and $d_i = a_i c_i + b_i$, $i = 1, \ldots, N-1$. Since P_{RD} is a RV, the probability of incidence $x = \varpi d_{N-1}$ is equal to zero. When the value x satisfies $\frac{x}{\varpi} \in [d_{i-1}, d_i]$ with $i = 1, 2, \ldots, N-1$, eq. (24) can be simplified, based on (5), to

$$\begin{aligned} F^c_{P_{RD}}(x) &= \Pr\{P_{RD} \geq x\} \\ &= \Pr\left\{\|\boldsymbol{h}_{SR}\|^2 \geq \frac{1}{a_i p_{SR}}\left(\frac{x}{\varpi} - b_i\right)\right\} \\ &= \Pr\left\{\frac{1}{a_i}\left(\frac{x}{\varpi}\right) \leq p_{SR}\left\|\boldsymbol{h}^2_{SR}\right\| < c_i\right\} \\ &\quad + \sum_{n=i+1}^{N} \Pr\left\{a_n p_{SR}\left\|h^2_{SR}\right\| + b_n \geq \frac{x}{\varpi}, c_{n-1} \leq p_{SR}\left\|h^2_{SR}\right\| \leq c_n\right\}\right\} \\ &= \Pr\left\{\left\|h^2_{SR}\right\| \geq \frac{1}{a_i p_{SR}}\left(\frac{x}{\varpi} - b_i\right)\right\} \end{aligned} \quad (25)$$

Noting that $\|\boldsymbol{h}_{SR}\|^2$ is noncentral chi-squared distributed, the CCDF of P_{RD} is

$$F^c_{P_{RD}}(p) = Q_{m_1 N_S}\left(\lambda_{SR}\sqrt{\frac{2m_1}{\Omega_{SR}}}, \sqrt{\frac{2m_1}{a_i p_{SR}\Omega_{SR}}\left(\frac{x}{\varpi} - b_i\right)}\right), \quad x \in \left[\varpi d_{i-1}, \varpi d_i\right] \quad (26)$$

APPENDIX B
PROOF OF CCDF FOR ART

The CCDF of the transmission power for the sensor, P_{RD}, is

$$\begin{aligned} F^c_{P_{RD}}(x) &= \Pr\left\{\varpi P^{ArT}_{EH}\left(p_{SR}\|\boldsymbol{h}_{SR}\|^2\right) \geq x\right\} \\ &= \Pr\left\{\|\boldsymbol{h}_{SR}\|^2 \geq \frac{1}{b_0 p_{SR}} \tanh^{-1}\left(\frac{x}{\varpi a_0}\right)\right\}. \end{aligned} \quad (27)$$

We then express $\tanh^{-1}(\cdot)$ in terms of the natural logarithm, $\ln(\cdot)$, while noting that $\|\boldsymbol{h}_{SR}\|^2$ is noncentral chi-squared distributed, to give a CCDF of P_{RD} in the form of

$$F^c_{P_{RD}}(x) = Q_{m_1 N_S}\left(\lambda_{SR}\sqrt{\frac{2m_1}{\Omega_{SR}}}, \sqrt{\frac{m_1 B}{b_0 \Omega_{SR} p_{SR}}}\right). \quad (28)$$

REFERENCES

[1] H. Elahi, M. Eugeni, and P. Gaudenzi, *Piezoelectric Aeroelastic Energy Harvesting*, 1st ed. Amsterdam, The Netherlands: Academic, 2022.

[2] X. Wang, *Frequency Analysis of Vibration Energy Harvesting Systems*, 1st ed. Amsterdam, The Netherlands: Academic, 2016.

[3] S. M. Walsh and M. S. Strano, *Robotic Systems and Autonomous Platforms*, 2nd ed. Amsterdam, The Netherlands: Academic, 2019.

[4] S. H. Lee, R. Zhang, and K. B. Huang, "Opportunistic wireless energy harvesting in cognitive radio networks," *IEEE Trans. Wireless Commun.*, vol. 12, no. 9, pp. 4788–4799, Sep. 2013.

[5] P. N. Alevizos and A. Bletsas, "Sensitive and nonlinear far-field RF energy harvesting in wireless communications," *IEEE Trans. Wireless Commun.*, vol. 17, no. 6, pp. 3670–3685, Jun. 2018.

[6] H. Azarhava and J. M. Niya, "Energy efficient resource allocation in wireless energy harvesting sensor networks," *IEEE Wireless Commun. Lett.*, vol. 9, no. 7, pp. 1000–1003, Jul. 2020.

[7] H. Ju and R. Zhang, "Throughput maximization in wireless powered communication networks," *IEEE Trans. Wireless Commun.*, vol. 13, no. 1, pp. 418–428, Jan. 2014.

[8] S. Sudevalayam and P. Kulkarni, "Energy harvesting sensor nodes: Survey and implications," *IEEE Commun. Surveys Tuts.*, vol. 13, no. 3, pp. 443–461, 3rd Quart., 2011.

[9] R. Zhang and C. K. Ho, "MIMO broadcasting for simultaneous wireless information and power transfer," *IEEE Trans. Wireless Commun.*, vol. 12, no. 5, pp. 1989–2001, May 2013.

[10] L. Liu, R. Zhang, and K.-C. Chua, "Multi-antenna wireless powered communication with energy beamforming," *IEEE Trans. Commun.*, vol. 62, no. 12, pp. 4349–4361, Dec. 2014.

[11] Y. Ma, H. Chen, Z. Lin, Y. Li, and B. Vucetic, "Distributed and optimal resource allocation for power beacon-assisted wireless-powered communications," *IEEE Trans. Commun.*, vol. 63, no. 10, pp. 3569–3583, Oct. 2015.

[12] W. Huang, H. Chen, Y. Li, and B. Vucetic, "On the performance of multiantenna wireless-powered communications with energy beamforming," *IEEE Trans. Veh. Technol.*, vol. 65, no. 3, pp. 1801–1808, Mar. 2016.

[13] Y. Liu, "Wireless information and power transfer for multirelay-assisted cooperative communication," *IEEE Commun. Lett.*, vol. 20, no. 4, pp. 784–787, Apr. 2016.

[14] S. Ladan and K. Wu, "Nonlinear modeling and harmonic recycling of millimeter-wave rectifier circuit," *IEEE Trans. Microw. Theory Techn.*, vol. 63, no. 3, pp. 937–944, Mar. 2015.
[15] Z. Hameed and K. Moez, "Hybrid forward and backward threshold-compensated RF-DC power converter for RF energy harvesting," *IEEE Trans. Emerg. Sel. Topics Circuits Syst.*, vol. 4, no. 3, pp. 335–343, Sep. 2014.
[16] E. Boshkovska, D. W. K. Ng, N. Zlatanov, A. Kloelpin, and R. Schober, "Robust resource allocation for MIMO wireless powered communication networks based on a non-linear EH model," *IEEE Trans. Commun.*, vol. 65, no. 5, pp. 1984–1999, May 2017.
[17] Y. Dong, M. J. Hossain, and J. Cheng, "Performance of wireless powered amplify and forward relaying over Nakagami-*m* fading channels with nonlinear energy harvester," *IEEE Commun. Lett.*, vol. 20, no. 4, pp. 672–675, Apr. 2016.
[18] B. Clerckx and E. Bayguzina, "Waveform design for wireless power transfer," *IEEE Trans. Signal Process.*, vol. 64, no. 23, pp. 6313–6328, Dec. 2016.
[19] S. Wang, M. Xia, K. Huang, and Y. C. Wu, "Wirelessly powered two-way communication with nonlinear energy harvesting model: Rate regions under fixed and mobile relay," *IEEE Trans. Wireless Commun.*, vol. 16, no. 12, pp. 8190–8204, Dec. 2017.
[20] E. Boshkovska, D. W. K. Ng, N. Zlatanov, and R. Schober, "Practical non-linear energy harvesting model and resource allocation for SWIPT systems," *IEEE Commun. Lett.*, vol. 19, no. 12, pp. 2082–2085, Dec. 2015.
[21] M. Wagih, A. S. Weddell, and S. Beeby, "Millimeter-wave power harvesting: A review," *IEEE Open J. Antennas Propag.*, vol. 1, pp. 560–578, 2020.
[22] A. Olutayo, J. Cheng, and J. F. Holzman, "A new statistical channel model for emerging wireless communication systems," *IEEE Open J. Commun. Soc.*, vol. 1, pp. 916–926, 2020.
[23] K. Huang, C. Zhong and G. Zhu, "Some new research trends in wirelessly powered communications," *IEEE Wireless Commun.*, vol. 23, no. 2, pp. 19–27, Apr. 2016.
[24] D. Wang, F. Rezaei, and C. Tellambura, "Performance analysis and resource allocations for a WPCN with a new nonlinear energy harvester model," *IEEE Open J. Commun. Soc.*, vol. 1, pp. 1403–1424, 2020.
[25] N. C. Beaulieu and J. Xie, "A novel fading model for channels with multiple dominant specular components," *IEEE Wireless Commun. Lett.*, vol. 4, no. 1, pp. 54–57, Feb. 2015.
[26] P. T. Van, H.-H. N. Le, M.-D. N. Le, and D.-B. Ha, "Performance analysis in wireless power transfer system over Nakagami fading channels," in *Proc. Int. Conf. Electron., Inf., Commun.*, Jan. 2016, pp. 1–4.
[27] R. Morsi, D. S. Michalopoulos, and R. Schober, "Performance analysis of near-optimal energy buffer aided wireless powered communication," *IEEE Trans. Wireless Commun.*, vol. 17, no. 2, pp. 863–881, Feb. 2018.
[28] R. Morsi, E. Boshkovska, E. Ramadan, D. W. K. Ng, and R. Schober, "On the performance of wireless powered communication with non-linear energy harvesting," in *Proc. IEEE Workshop Signal Adv. Wireless Commun.*, Dec. 2017, pp. 1–5.
[29] A. K. Shukla, V. Singh, P. K. Upadhyay, A. Kumar, and J. M. Moualeu, "Performance analysis of energy harvesting-assisted overlay cognitive NOMA systems with incremental relaying," *IEEE Open J. Commun. Soc.*, vol. 2, pp. 1558–1576, 2021.
[30] T. M. Hoang, B. C. Nguyen, P. T. Tran, and L. T. Dung, "Outage analysis of RF energy harvesting cooperative communication systems over Nakagami-*m* fading channels with integer and non-integer *m*," *IEEE Trans. Veh. Technol.*, vol. 69, no. 3, pp. 2785–2801, Mar. 2020.
[31] T. Le, K. Mayaram, and T. Fiez, "Efficient far-field radio frequency energy harvesting for passively powered sensor networks," *IEEE J. Solid-State Circuits*, vol. 43, no. 5, pp. 1287–1302, May 2008.
[32] A. Olutayo, H. Ma, J. Cheng, and J. F. Holzman, "Level crossing rate and average fade duration for the Beaulieu-Xie fading model," *IEEE Wireless Commun. Lett.*, vol. 6, no. 3, pp. 326–329, Jun. 2017.
[33] E. W. Weisstein. "Marcum Q-function." 1999. [Online]. Available: http://mathworld.wolfram.com/MarcumQFunction.html
[34] I. S. Gradshteyn and I. M. Ryzhik, *Table of Integrals, Series, and Products*, 6th ed. New York, NY, USA: Academic, 2000.